Electrochemical Iron Recovery from Biologically Produced Magnetite via Iron Oxide/Hydroxide Conversion: First Steps towards Terrestrial and Martian Applications

Reza Fayaz[1,5,6], Antoine Carissimo[3,5,6], Md Izzuddin Jundullah Hanafi[4,5], Guillaume Pillot[3,5,6], Michael Baune[1,6], Thorsten M. Gesing[4,5], Sven Kerzenmacher[3,5,6], Fabio La Mantia[2,5,6] & Jorg Thöming[1,5,6]*

[1]University of Bremen, Chemical Process Engineering Group (CVT), Leobener Strasse 6, 28359 Bremen, Germany
[2]University of Bremen, Energy Storage and Conversion Systems, Wiener Strasse 12, 28359 Bremen, Germany
[3]University of Bremen, Environmental Process Engineering Group (UVT), Leobener Strasse 6, 28359 Bremen, Germany
[4]University of Bremen, Institute of Inorganic Chemistry and Crystallography, Leobener Strasse 7, 28359 Bremen, Germany
[5]University of Bremen, MAPEX Center for Materials and Processes, Bibliothekstrasse 1, 28359 Bremen, Germany
[6]University of Bremen, Center for Environmental Research and Sustainable Technology (UFT), Leobener Strasse 6, 28359 Bremen, Germany
*Email: thoeming@uni-bremen.de

Abstract

Ferrihydrite ($Fe_{10}O_{14}(OH)_2$), an iron oxide/hydroxide, is found in a variety of terrestrial and extraterrestrial environments. This study presents a novel approach that combines bio-mineralization and electrolysis for the efficient mining of low-grade iron resources. Iron-reducing *Carboxydothermus ferrireducens* bacteria converted an iron oxide/hydroxide Fe(III)-mixture to magnetite. This ferrimagnetic phase was magnetically extracted and subsequently electrolyzed at 363 K in an alkaline medium to produce metallic iron. Integrating a heat treatment step increased the iron yield to 67 %. This resulted in a high current efficiency of 63% and an energy consumption of 19.1 MJ/kg, which is competitive with current pyrometallurgical practices. Heat-induced morphological and chemical changes facilitated iron reduction and suppressed parasitic hydrogen evolution.
Furthermore, improved reducibility of the biomineralized material was observed. This method could facilitate the exploitation of marginal iron reserves, particularly in areas where no rich ores are available. The process also promises adaptation to extraterrestrial sources such as the Martian regolith.

Graphical Abstract

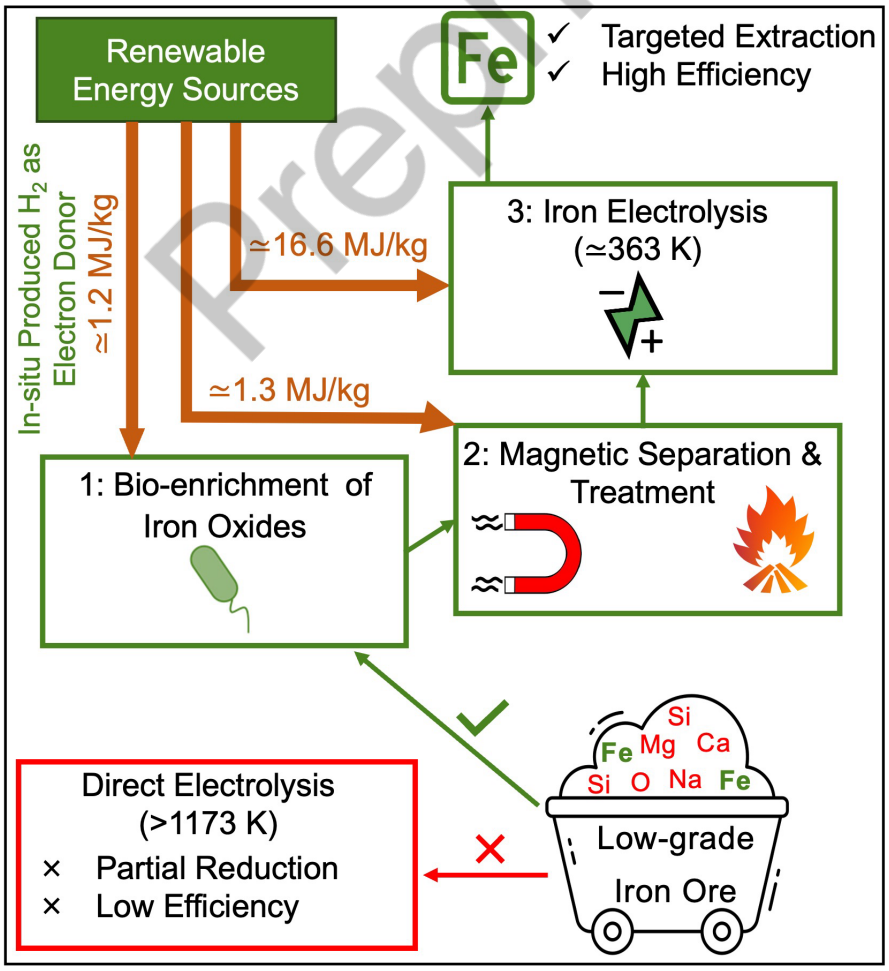

Keywords

Iron production, Bio-mineralization, Electrochemical reduction, Low-grade ore beneficiation, Extraterrestrial mining, In-situ resource utilization (ISRU)

1. Introduction

Metallic iron, Fe(0), is a valuable material globally, and its demand is expected to continue to rise [1]. The traditional process of smelting iron with coke produces significant emissions of greenhouse gases and a high turnover of energy [2], so finding environmentally friendly alternatives is crucial [3]. While hydrogen is widely used for direct iron reduction processes [4], electrochemical reduction has also been proposed to replace current polluting methods [5,6,7]. However, most efforts to date have concentrated on high-value resources, and innovations that can utilize currently unusable iron resources may have significant economic and strategic implications in the future.

Especially for such currently unusable iron resources like low-grade ores, traditional iron extraction methods pose challenges to the Sustainable Development Goals (SDGs) [8], including SDG 13 (Climate Action) and SDG 7 (Affordable and Clean Energy). Based on the utilization of renewable energy and electrochemistry to support SDG 12 (Responsible Production) [9], this paper presents a concept for converting low-grade iron ore (bio-) electrochemically into iron. This concept also offers the possibility of extracting iron on Mars using locally available materials and renewable energy sources. Thereby, it complements established in-situ resource utilization (ISRU) methods, such as MOXIE [10], which produces oxygen from CO_2 on Mars.

Ferrihydrite, an iron oxide/hydroxide with variable iron content, occurs predominantly as an amorphous phase in sands, sediments, and laterites [11]. It is also a major component of Fe-rich sludges derived from water treatment plants and mining and ore processing industries [12]. This iron oxide/hydroxide is not normally targeted for iron extraction due to its amorphous nature and association with various impurities. Given the future depletion of high-grade iron ore reserves, alternative approaches are being sought to convert low-grade ores into useful products. The bio-mineralization of these underutilized resources could play a role in their future use [13].

In addition, iron fabrication using ISRU-generated electricity as the power source is crucial for future Mars exploration and habitation [14,15]. Martian regolith contains several metal oxides, including iron-bearing phases like ferrihydrite [16], but its complex mineralogy makes direct electrolysis challenging. Current methods, such as molten regolith electrolysis (MRE), operate at extreme temperatures (~1873 K) and result in partial reductions and mixed metallic mixtures [17,18]. Solid-state reduction at relatively lower temperatures (~1173 K) also struggles with incomplete oxygen removal and unselective metal extraction [19]. Given these limitations, pre-concentrating iron oxides from regolith would simplify the process and enable more efficient, lower-temperature electrolysis, reducing complexity and energy requirements.

Iron oxides exhibit semiconducting properties, making direct electroreduction challenging [20]. However, solid-state deoxidation electrolysis of hematite (Fe_2O_3) [5] and magnetite (Fe_3O_4) [21] has been successfully achieved in an aqueous medium at a moderate temperature of 363 K. In this process, iron oxides are reduced to metallic iron in an electrolytic cell. A pure iron oxide pellet is the cathode, submerged in a highly alkaline solution. During the reduction, iron ions are converted to metallic iron at the cathode, while oxygen ions are expelled and migrate to the anode, where they are released as oxygen gas [6,7].

The electrochemical reduction of iron oxides can proceed via two coexisting mechanisms: (i) a dissolution-reduction pathway, where Fe(III) dissolves to form soluble complexes (e.g., $Fe(OH)_4^-$), which are then stepwise reduced to metallic iron; and (ii) a solid-state reduction mechanism, where oxygen ions are directly removed from the oxide lattice and transported through the electrolyte [5]. A study [22] indicated that hematite displays higher reducibility and current efficiency in electrochemical reduction compared to magnetite, which suffers from slower reduction kinetics and lower efficiency due to side reactions such as hydrogen evolution. The hydrogen evolution reaction (HER) occurs in alkaline electrolysis regardless of the iron oxide used as a cathode. In the case of magnetite, the HER is more likely to be pronounced due to the need for higher cathodic potentials, which are closer to the potential for hydrogen evolution.

However, this electrochemical process is sensitive to impurities in the feedstock. Studies on $Fe_{2.3}Mg_{0.7}O_4$ spinel [23], red mud [24], and pseudobrookite (Fe_2TiO_5) [25] have shown that impurities such as Mg, Si, Al, and Ti significantly hinder the efficiency of the process by blocking electrochemically active sites and reducing the current efficiency of any ionic iron species. These findings highlight the detrimental effects of impurities on direct electroreduction. Although electrolytic iron recovery from red mud in alkaline media has been demonstrated, it requires aggressive chemical pretreatment [26]. To contribute to overcoming this challenge, this research explores bio-enrichment as a feasible approach for future iron recovery strategies. The biological conversion of ferric oxide to magnetically responsive forms could allow selective concentration of iron and separation of impurities before electrolysis, thereby mitigating the negative effects of impurities and improving process efficiency.

Bio-mining uses biological systems, usually microorganisms, to extract and recover valuable metals from ores and waste materials [27]. It holds the potential for ISRU, but the technology is still in its infancy [28]. A series of biomining experiments conducted on board the International Space Station (ISS) demonstrate that the process is

effective regardless of gravity conditions [29]. Recently, a novel biomining approach based on bio-mineralization and magnetic extraction has been conceptualized and evaluated as promising [30]. It relies on the ability of iron-reducing microorganisms to bio-mineralize magnetite during the reduction of ferric iron oxides, a naturally occurring process in sediments [13]. To the best of our knowledge, this biomineralization approach has only been experimentally tested once with Martian and Lunar simulants, leading to a significantly increased iron extraction, thereby highlighting its potential for ISRU [31]. However, this biological process does not convert the iron to Fe(0).

In this study, we demonstrate the potential advantage of bio-mineralization in enriching low-grade iron ores to make them more suitable for electrochemical reduction. First, iron-reducing bacteria convert iron-bearing phases into magnetically responsive bio-magnetite. The bio-mineralization Fe(II)/Fe(III) mineral is then reduced to Fe(0) by electrolysis. An intermediate heat treatment step is introduced to increase iron yield further and reduce energy consumption. The improved reducibility of bio-mineralized materials suggests a promising route for economically viable iron extraction. This approach also offers a practical solution for extraterrestrial environments such as Mars, where conventional extraction methods are not feasible.

2. Materials and methods

2.1. Electrode materials

Various iron-based materials were used as cathodes in this study, including (i) synthesized iron oxide/hydroxide, (ii) bio-magnetite produced via microbial reduction, (iii) bio-hematite formed by thermal oxidation of bio-magnetite (under air at 1173 K for 3 h), and (iv) commercial hematite (Carl Roth, ≥ 95 %, 400 mesh) and magnetite (Thermo Scientific, ≥ 97 %, 325 mesh). The iron oxide/hydroxide was prepared by gradually adding NaOH 10 M in a solution of $FeCl_3 \cdot H_2O$ (108 g/L) until the pH stabilized at 7. The iron oxide/hydroxide suspension was then centrifuged and washed with deionized water.

For cathode pellet formation, a conductive Ag-paste (MG Chemicals, product code: 8330S-A) was used for pelletization to replace the commonly used sintering, which causes mineral phase alteration of precursors. Approximately 1 g of powder produced each disk-shaped pellet (diameter: 10 mm, thickness: 3 mm). Around 2 mL of glue was applied to each pellet and cured at 353 K for 2 h.

Electrolysis was performed using samples containing only Ag paste to account for the potential effect of silver epoxy on the electrochemical measurements. Initially, it was confirmed that silver was not involved in the electrochemical reaction, as no phase change was observed post-electrolysis (confirmed by X-ray powder diffraction (XRPD) analysis). The charge resulting from this control experiment was measured (2420 C for 20 h) and subtracted from the total electrical charge obtained from the main electrolysis experiments. This ensured that the HER associated with silver was excluded from the calculations.

A Martian regolith simulant, MGS-1 (Space Resource Technologies (SRT), batch code: 002-05-001-0621, mean particle size: 90 μm) was also analyzed to understand the mineral composition and identify the iron-containing phases.

2.2. Bio-mineralization

Bio-magnetite was prepared by providing this iron oxide/hydroxide to *Carboxydothermus ferrireducens*, an iron-reducing bacterium, as the terminal electron acceptor for anaerobic respiration. *C. ferrireducens* was purchased from DSMZ (DSM 11255). It is a thermophile (323 to 347 K) and a facultative autotroph, isolated from hot springs in Yellowstone National Park, Wyoming, USA. To simplify cultivation, the bacterium was cultivated organoheterotrophically with glycerol as the carbon and energy source. It was cultivated anaerobically in 1 L Schott bottles.

The medium contained, per liter of deionized water: 0.33 g of KH_2PO_4, 0.33 g of NH_4Cl, 0.33 g of KCl, 0.33 g of $MgCl_2 \cdot 6H_2O$, 0.33 g of $CaCl_2 \cdot 2H_2O$, 0.2 g of $MgSO_4 \cdot 7H_2O$, 2.5 g of $NaHCO_3$, 0.1 g of yeast extract, and 1 mL of Wolfe's mineral elixir (trace elements solution, DSMZ). All chemicals were > 99 % pure and purchased from Carl Roth (Germany), Merck (Germany), or VWR International (United States). The medium was prepared in an anaerobic chamber, adjusted to pH 6.8 with 1 M HCl, and autoclaved. $CaCl_2 \cdot 2H_2O$ was added to the medium after autoclaving, from an autoclaved concentrated solution. The trace elements solution contained, per liter of deionized water: 30 g of $MgSO_4 \cdot 7H_2O$, 5 g of $MnSO_4 \cdot nH_2O$, 10 g of NaCl, 1 g of $FeSO_4 \cdot 7H_2O$, 1.8 g of $CoCl_2 \cdot 6\ H_2O$, 1 g of $CaCl_2 \cdot 2H_2O$, 1.8 g of $ZnSO_4 \cdot 7H_2O$, 0.1 g of $CuSO_4 \cdot 5H_2O$, 0.18 g of $AlK(SO_4)_2 \cdot 12H_2O$, 0.1 g of H_3BO_3, 0.1 g of $Na_2MoO_4 \cdot 2H_2O$, 2.8 g of $(NH_4)_2Ni(SO_4)_2 \cdot 6\ H_2O$, 0.1 g of $Na_2WO_4.2H_2O$, and 0.1 g of Na_2SeO_4. The salts were dissolved after adjusting the pH to 1.0 with sulfuric acid. The medium was distributed to three 1 L cultivation bottles containing 500 mL of medium. After autoclaving, the cultivation bottles were complemented with glycerol (40 mM), iron oxide/hydroxide (100 mM of Fe^{3+}), and $Na_2S \cdot 9H_2O$ (0.05 mM of Na_2S) from concentrated solutions. The glycerol-concentrated solution was autoclaved while the $Na_2S \cdot 9H_2O$ solution was filter-sterilized. Iron oxide/hydroxide was not autoclaved to prevent crystallization. The cultivation bottles were inoculated with 8 mL of iron oxide/hydroxide-reducing *Carboxydothermus* cultures, and placed in an incubator (Heratherm, Thermo Fisher Scientific, USA) at 338 K and magnetically stirred at 400 rpm for about 48 h until the particles in the

medium became black and magnetic. The concentration of Fe^{2+} was measured spectrophotometrically with the ferrozine assay [32]. Before measurements, 1 mL of the sample was mixed with 1 mL of 4 M HCl until the particles were visually dissolved (less than an hour to a few days for the final samples with black magnetic particles). Cells were observed during cultivation under a fluorescence microscope. Liquid samples were stained with 2 µg/mL of 4′,6-diamidine-2-phenylindole (DAPI) (Carl Roth, Germany), illuminated with ultraviolet light (385 nm), and observed with a Zeiss Microscope Axioscope 7 (Carl Zeiss, Germany) at 500x magnification (reflected light at 465 nm). At the end of cultivation, the magnetic particles were rinsed with deionized water once and dried at room temperature. In total, about 14 g of black magnetic particles were obtained from the 3 cultures.

2.3. Electrochemical experiments

Electrical contacts were established by connecting a Kanthal® wire to a hole in the center of the cathode pellet. An anion exchange membrane (Reichelt Chemietechnik, MA-3475) was employed to separate the electrodes. Before each test, the membrane was activated by immersing it in a 10 % salt solution at 328 K for 3 h. Anion exchange membrane (AEM) was employed to physically separate the anode and cathode compartments to suppress parasitic effects such as gas crossover and redox cycling of carbon species, as shown in our earlier work [5]. The electrochemical tests were conducted in a Teflon H-cell. An electrolyte solution was prepared by dissolving 10 M NaOH (VWR, 99.3 %) in water. This highly concentrated electrolyte solution should minimize the hydrogen evolution reaction (HER) and reduce water loss [33].
The working electrode consisted of iron oxide/hydroxide, bio-magnetite, bio-hematite, commercial magnetite, or commercial hematite pellets connected to the wire.
A commercial Ag|AgCl|KCl (3.5 M) reference electrode (Xylem Analytics, +0.205 V vs. SHE) was used, specifically designed to withstand alkaline conditions and ensure stable performance in high-pH electrochemical environments. Based on insights from our prior study [5], we employed Ni/Fe as a non-contaminating inert counter electrode, which also catalyzes oxygen evolution and reduces the anodic overpotential [34]. This anode electrode was a rod-shaped Ni36/Fe64 alloy, with a diameter of 20 mm and a height of 100 mm. The measurement equipment employed was a potentiostat (IPS Elektroniklabor, PGU-1A-OEM). Before conducting electrochemical tests, the cathode electrodes were immersed in the electrolyte (10 M NaOH with a pH of 15 for both anolyte and catholyte) for 30 minutes to ensure proper wetting.
To screen electrochemical redox peaks at the hematite/electrolyte interface, cyclic voltammetry (CV) tests were performed. The CVs were recorded with a scan rate of 50 mV/s, within a range of -1.8 V to +0.5 V relative to the open circuit potential. They were repeated for 3 cycles. Electrolysis tests (chronoamperometry) were conducted by applying a constant potential of -1.4 V vs. the Ag/AgCl reference electrode for 20 or 5 h while measuring the corresponding current. A second potentiostat (IPS Elektroniklabor, IMP 83 PC T-BC) was employed to measure the total cell voltage during electrolysis for energy calculations. All electrochemical tests were conducted in an argon-protected atmosphere to suppress the carbon parasitic reaction loop [5]. All electrochemical tests were replicated at least three times.

2.4. Sample characterization

After the reduction process, the electrodes were pulled above the electrolyte line and dried under argon. They were pulled out after the cell cooled. To eliminate any residual electrolyte, the cathode samples were subjected to Soxhlet extraction with water as the solvent for up to 5 h [35]. Subsequently, the samples were dried in an oven at 80 °C for 1 h and weighed. To characterize the samples, they were ground and subjected to XRPD analysis [36]. XRPD measurements were carried out on a Bruker D8 Discover diffractometer using CuKα1,2 radiation ($\lambda_{K\alpha1}$ = 154.05929(5) pm, $\lambda_{K\alpha2}$ = 154.4414(2) pm) in Bragg-Brentano geometry. Data was collected at ambient conditions in a range of 20° to 100° 2θ, with a step width of 0.0149° 2θ and a measurement time of 0.3 seconds per step using an energy-discriminating LynxEye-XET multi-strip detector. The Rietveld refinements were performed using TOPAS V6.0 (Bruker AXS). The average crystallite size of the amorphous scattering samples was determined using the EnvACS approach [37]. For elemental mapping of selected sponges produced, scanning electron microscopy (SEM, Device: JEOL, JMS-6510) and energy dispersive X-ray spectrometer (EDX, Device: Bruker, XFlash 410-M) analyses were performed. The specific surface area of the sample was measured using a Brunauer-Emmett-Teller (BET) surface area analyzer, Belsorb Mini (Microtrac), with N_2 as an adsorption gas. Samples were pre-treated at 393 K for 3 h in a vacuum.

3. Results and discussion

3.1. Bio-mineralization of magnetite and conversion to hematite

Ferrihydrite, an iron-rich component of various natural soils, industrial wastes, and Martian regolith, is classified as an iron oxide/hydroxide. In this study, we synthesized a chemically similar compound to serve as the starting material. This compound was selected for its ability to support microbial respiration under anoxic conditions. Due to the variable iron content and amorphous nature of ferrihydrite, we could not confidently confirm the identity of

our synthesized material as ferrihydrite. We referred to it instead as 'iron oxide/hydroxide'.
Bio-magnetite was produced by supplying this iron oxide/hydroxide to the iron-reducing bacterium *C. ferrireducens* as the terminal electron acceptor for anaerobic respiration. That is, the synthesized iron oxide/hydroxide was included in the cultivation medium of *C. ferrireducens*, which couples the oxidation of glycerol with the reduction of ferric iron oxide/hydroxide to support its metabolism (anaerobic respiration) [38]. Upon reduction of the Fe(III) cations into Fe(II), the iron oxide/hydroxide was transformed into magnetite, a mixed-valent mineral. The concentration of Fe(II), measured spectrophotometrically after extraction in HCl, increased over time, reaching about 35 % of Fe(III) reduction after two days of cultivation (Fig. 1a) A black magnetic material was formed and identified as magnetite using X-ray powder Bragg-Rietveld (XRPD) data (refer to electronic supplementary material, Supplementary Fig. S-2). Microbial cells were observed at the surface of the particles (Fig. 1a). These results align with what was previously reported for this iron-reducing species [37,38].
In this study, glycerol was used as a carbon and energy source for bacterial cultivation. On Mars, however, organic carbon could be produced using cyanobacteria, which fix carbon from CO_2 without relying on carbohydrate feedstocks [39,40]. Additionally, some (hyper)thermophilic iron-reducing microorganisms (IRM), including *C. ferrireducens* [42], can function as facultative lithoautotrophs [43], utilizing only inorganic sources like H_2 and CO_2, making them suitable for cultivation without organic carbon.
Magnetite bio-mineralization by IRM typically occurs at circumneutral pH levels, around 7, where these neutrophilic microorganisms thrive. They can grow and reduce iron across a wide temperature range, from -2°C to 121°C [43,44], and are categorized as psychrophiles, mesophiles, thermophiles, or hyperthermophiles based on their optimal growth temperatures.

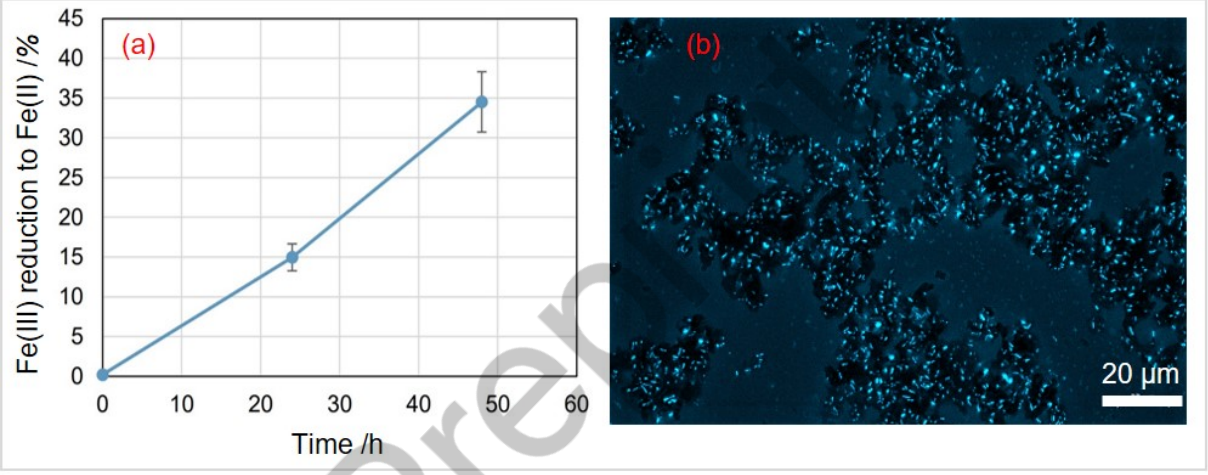

Fig. 1: Growth of the iron-reducing bacterium with iron oxide/hydroxide. (a) The ratio of Fe(II) produced to the initial Fe(III) concentration, as a function of time. The average for three cultures is shown, with error bars indicating the standard deviation. (b) Black magnetic particles from *C. ferrireducens* cultures (2 days) were observed with fluorescent light, revealing the presence of microbial cells (blue) all over the particles.

The process diagram (Fig. 2) illustrates the preparation of three different iron-based materials for alkaline electrolysis. It begins with iron oxide/hydroxide, which undergoes microbial reduction to produce bio-magnetite. This bio-magnetite can either be used directly or further processed through heat treatment (1173 K, 3 h, under air) to examine the effects of chemical and microstructural alterations on electrochemical behavior. All three materials, iron oxide/hydroxide, bio-magnetite, and the heat-treated product, are then pelletized. These pellets serve as cathodes in an alkaline electrolysis setup operating with a 10 M NaOH solution at 363 K. Each pellet undergoes cathodic reduction at -1.4 V vs. Ag/AgCl for conversion to Fe(0).
X-ray powder diffraction refinements (Supplementary Fig. S-2) and Brunauer-Emmett-Teller (BET) analyses revealed changes in the crystal structure induced by bio-mineralization and heat treatment. Bio-mineralization reduced the specific surface area (SSA) from 285 m^2/g for the iron oxide/hydroxide to 41.5 m^2/g for bio-magnetite. XRPD data also confirm that bio-mineralization successfully converted a quantum-crystalline iron oxide/hydroxide with an average crystallite size (ACS) of 2.7(1) nm into a micro-crystalline bio-magnetite with an ACS of 16.2(2) nm (Table 1). Due to its high diffuse scattering content, the ACS of iron oxide/hydroxide could only be determined using the PDF EnvACS method [37] (Supplementary Fig. S-3). This transformation can be explained by bacterial metabolic activities, and bacterial structures such as cell walls, membranes, or debris act as nucleation points for crystallization [45,46].
XRPD also confirmed the full oxidation of bio-magnetite (Fe(II)/Fe(III)) to a single (Fe(III)) phase ('bio-hematite') via heat treatment. The heat consumes the oxygen released from the bio-magnetite during the bio-mineralization phase. Following this, the SSA further declined to 0.27 m^2/g for bio-hematite, accompanied by an increase in the degree of crystallinity (DC) to 96(5) % and the ACS to 238(6) nm). The numbers in brackets represent the estimated standard deviations of the obtained values in the last digit.

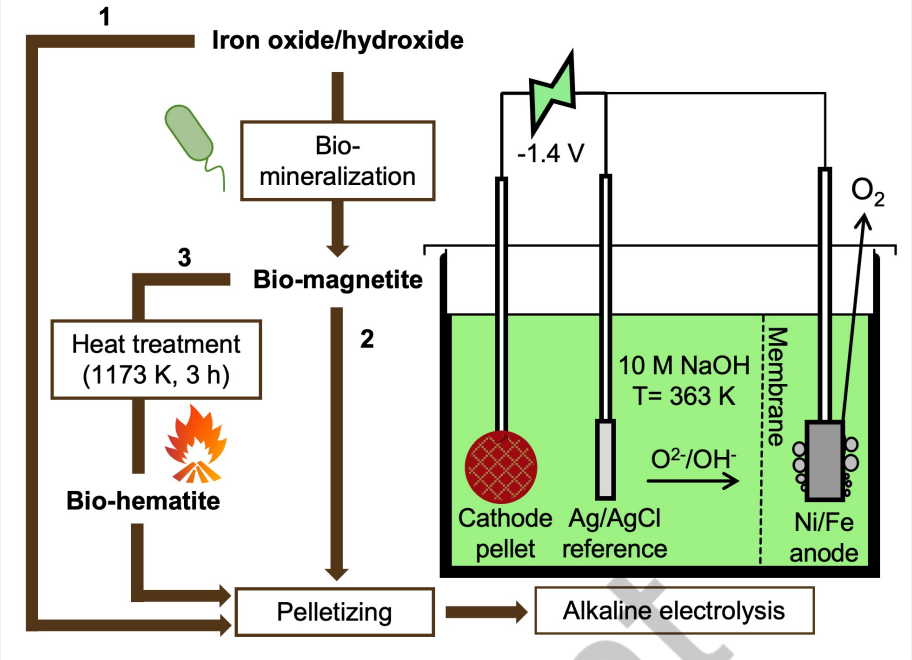

Fig. 2: Schematic of bio-magnetite production from iron oxide/hydroxides, pelletizing with optional heat treatment, and subsequent electrochemical conversion to metallic iron at 363 K in alkaline electrolysis using a two-compartment cell separated by an anion exchange membrane. Final pellet characterization followed.

Table 1. The degree of crystallinity (DC), average crystallite size (ACS), and specific surface area (SSA) of the various feedstocks. The numbers in brackets are the estimated standard deviations of the obtained values in the last digit. (*) XRPD data of iron oxide/hydroxide shows broad humps associated with the quantum-crystalline phase which makes it impossible to distinguish the amorphous content.

Sample	DC /wt.%	ACS /nm	SSA /(m^2/g)
Iron oxide/hydroxide	*	2.7(1)	285
Bio-magnetite	80(5)	16.2(2)	41.5
Commercial magnetite	87(5)	74(1)	8.1
Bio-hematite	96(5)	238(6)	0.27
Commercial hematite	95(5)	135(1)	2.6
Heat-treated commercial hematite	99(5)	173(2)	0.76

3.2. Comparative electrochemical analysis

To observe the changes caused by bio-mineralization and heat treatment on the electrochemical process of iron reduction, CV and chronoamperometry tests were conducted for the starting iron oxide/hydroxide, bio-magnetite, and bio-hematite.

In the first CV cycles, the plots for the three materials tested are superimposed, with no discernible redox peaks (Supplementary Fig. S-4), indicating that the iron oxide surfaces had not yet reached electrochemical activity. This initial lack of activity is consistent with the need for surface conditioning, where repeated cycling activates the material and enhances electron transfer. However, clear electrochemical behavior is apparent in the third CV cycle (Fig. 3a). The cathodic current peak at approximately -1.3 V vs. Ag/AgCl reference electrode is attributed to iron oxide reduction to iron. For iron oxide/hydroxide and bio-magnetite, the reduction peaks occur earlier than for bio-hematite and exhibit higher cathodic currents. The parasitic HER starts in all samples shortly after the reduction peak for Fe(0) formation. However, the onset of HER shows higher cathodic currents in bio-magnetite and the highest currents in iron oxide/hydroxide.

In addition, whereas there is a more pronounced boundary between the iron and HER peaks for bio-hematite, these appear to be more disruptive for iron oxide/hydroxide and bio-magnetite. During the anodic sweep, the corresponding anodic currents are higher for bio-magnetite, possibly due to high capacitive currents [48] or, more

likely, due to superimposed Faradaic currents such as the re-oxidation of hydrogen potentially trapped in the microstructure.
Consequently, electrolysis tests were conducted by applying a potential of -1.4 V vs. Ag/AgCl for 20 h. It should be noted that the application of a potential of -1.3 V vs. Ag/AgCl did not result in any reduction of iron cations. Likely, overcompensation for the mass transfer resistance caused by limiting diffusion in boundary layers is required. The corresponding electrolysis currents were measured over time (Fig. 3b), and the iron extraction yields were determined via XRPD. Monteiro et al. [21] demonstrated electrochemical reduction of magnetite at −1.15 V vs. Hg|HgO|NaOH (1 M) in 10 M NaOH at 90 °C, highlighting the strong influence of pellet porosity on iron yield. Our study employed a comparable setup at a slightly more negative potential (−1.4 V vs. Ag|AgCl|KCl 3.5 M), but focused on bio-mineralization and heat treatment to investigate how microstructural modifications affect electrochemical reducibility.

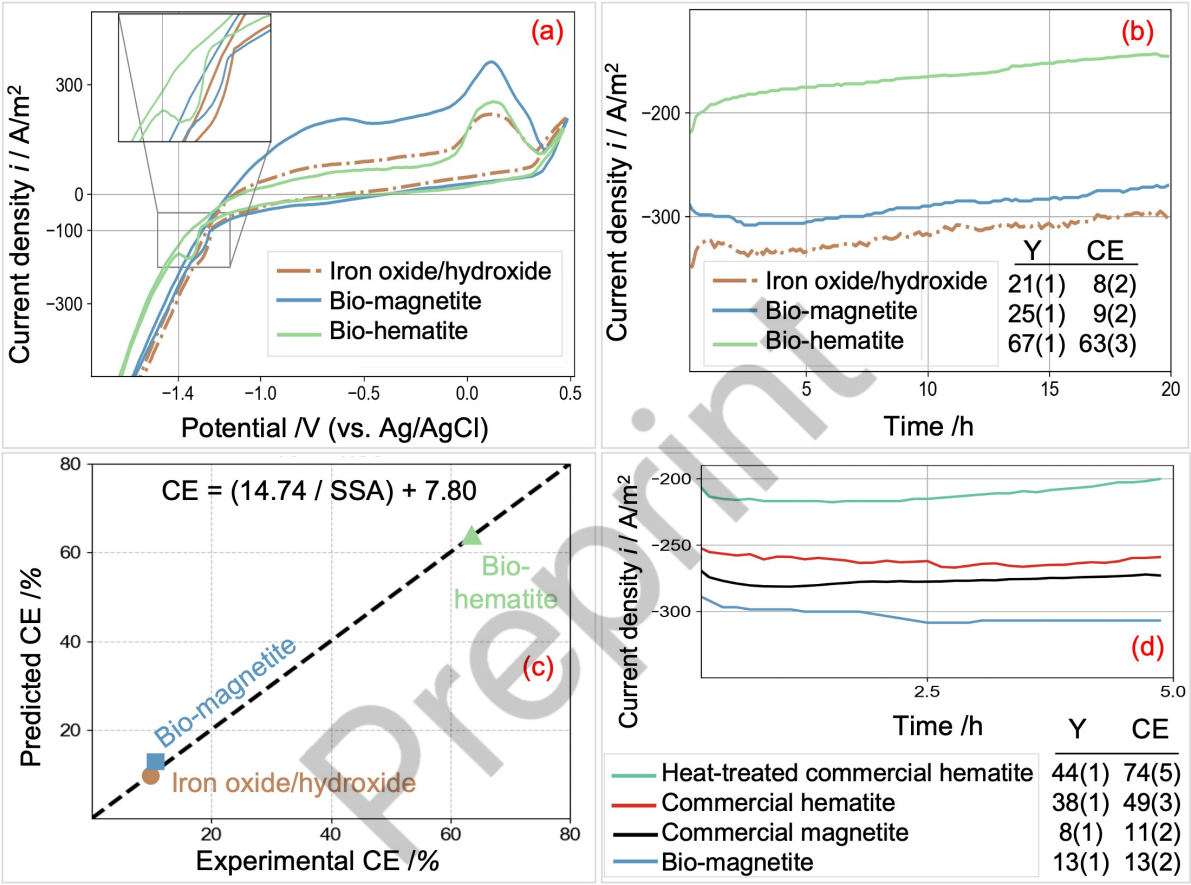

Fig. 3: Current densities during (a) the third cycle of cyclic voltammetry and (b) 20 h chronoamperometry at -1.4 V vs. Ag/AgCl in 10 M NaOH for iron oxide/hydroxide, biologically produced magnetite (bio-magnetite), and bio-hematite after additional heat treatment at 363 K; shown are also iron yields (Y) and current efficiencies (CE). (c) Parity plot illustrating the inverse correlation between current efficiency and specific surface area (SSA). (d) Comparison of reducibility: commercial hematite vs. heat-treated bio-hematite, and commercial magnetite vs. bio-magnetite by 5 h electrolysis, shown as iron yield (Y, wt.%) and current efficiency (CE, %). Numbers in brackets indicate estimated standard deviations (last digit). Note: 20 h tests (b) and 5 h tests (d) are not directly comparable due to different durations; 20 h tests focus on main materials, 5 h tests serve as controls.

The bio-hematite currents remain relatively low and with minimal fluctuations throughout the electrolysis, with an extracted iron yield of 67(1) wt.%. This stability is indicative of a steadier and efficient iron electrochemical reduction process. In contrast, iron oxide/hydroxide (yield: 21(1) wt.%) and bio-magnetite (yield: 25(1) wt.%) exhibit higher currents and fluctuations despite lower yields, suggesting a lower selectivity and a less desired reduction process. These observations can be attributed to thermodynamic and microstructural factors.
Thermodynamically, the standard Gibbs free energy required for further electrochemical decomposition to elemental iron reduces from 1013.7 kJ/mol for (Fe(II)/Fe(III)) oxides to 749.3 kJ/mol for Fe(III) oxides [49]. While the $Fe_2O_3 \rightarrow Fe_3O_4 \rightarrow Fe$ sequence is a known shrinking-core mechanism [50], the reduction of our heat-treated bio-magnetite (bio-hematite) appears to proceed via a direct $Fe_2O_3 \rightarrow Fe^0$ pathway, as XRPD analysis of partially reduced samples revealed no detectable magnetite phase.
Furthermore, with its higher average crystallite size, bio-hematite provides a crystal structure with reduced micro-

strain and bulk point defects that ensure pathways for electron movement that are more defined and less disrupted, which increases favorable iron reaction kinetics. The surface defects and morphology of iron oxide/hydroxide and bio-magnetite act as active sites for unwanted HER side reactions or inconsistent electron transfer. The higher SSA and the smaller ACS of iron oxide/hydroxide and bio-magnetite also mean greater surface-to-bulk volume, which increases the overall undesired electrochemical activity at the surface. Additionally, the dense magnetite shell causes lower diffusivity [51], supporting the formation of dense iron layers around the particle during the reduction, prohibiting further iron reduction, as it was also shown for the reduction of iron oxides with hydrogen [52].

An inverse relationship between current efficiency (CE) and SSA for all three minerals is observable as shown in Supplementary Fig. S-5. The parity plot (Fig. 3c) presents a model for predicting this correlation ($CE = 14.74 / SSA + 7.80$). The lower surface-to-bulk volume of bio-hematite means fewer active sites for parasitic HER and a more controlled contribution of electrons for iron reduction, with a high current efficiency of 63(3) %. In contrast, a higher surface area means more undesired electrochemical reactions, as the efficiency decreases to 8(2) % for iron oxide/hydroxide and 9(2) % for bio-magnetite.

Zhang et al. [53] showed that nanostructured iron oxides as electrode materials present challenges such as low thermodynamic stability and susceptibility to surface side reactions. Pervez et al. [54] additionally showed that the crystalline phases of iron oxide nanotubes demonstrated superior electrochemical performance compared to their amorphous counterparts. This enhanced behavior was attributed to the better-crystallized part of a phase providing a more defined path for ion diffusion and electron transport, as our results showed.

From a microstructural perspective, one might have anticipated that iron oxide/hydroxide would be much less efficient than bio-magnetite due to its SSA being about seven times higher. However, thermodynamics balances the scales, allowing more electrons to be dedicated to iron reduction. This is despite the abundance of active sites and side reactions. This is why iron oxide/hydroxide achieves a high yield and faradaic efficiency comparable to bio-magnetite. While no direct energy data for ferrihydrite electroreduction are available, Latta et al. [55] demonstrated its general reducibility in aqueous suspension via mediated electrochemical pathways under mild conditions.

The conversion of bio-hematite outperforms the other two materials regarding iron yield, current efficiency, voltage efficiency, and energy consumption (Fig. 4). The lower efficiency of non-heat-treated samples suggests that more electrical energy is diverted to non-productive processes. While bio-mineralization would act as a crucial upstream step in the extraction of iron oxide/hydroxides such as ferrihydrite from low-grade ore resources, intermediate oxidation using heat treatment is required to improve further electrochemical behavior.

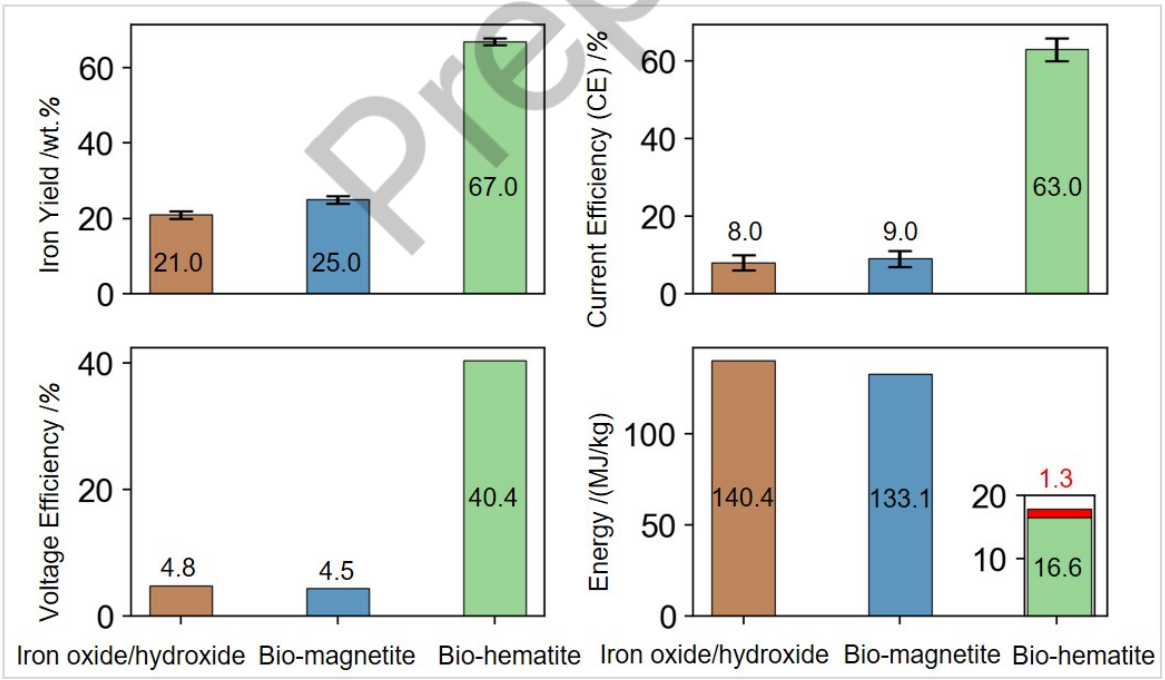

Fig. 4: Conversion of Fe(III)-oxide/hydroxide (ferrihydrite) to metallic iron with and without bio-enrichment to bio-magnetite and heat treatment to bio-hematite: iron extraction yield, current efficiency (CE), voltage efficiency, and energy consumption after 20 h electrolysis at -1.4 V vs. Ag/AgCl in 10 M NaOH at 363 K. The error bars indicate the standard deviation for the top two panels. For bio-hematite, the required energy is divided into the energy for electrolysis (16.6 MJ/kg) and the additional energy for heating to 1173 K for heat treatment. (1.3 MJ/kg).

In addition, bio-hematite requires a lower total cell voltage to maintain the applied cathodic potential, resulting in reduced electrolysis energy consumption and better voltage efficiency. Even considering the needed energy capacity for heating up to 900 °C for thermal treatment (1.3 MJ/kg) and microbial iron reduction energy (1.2 MJ/kg) [42], bio-hematite's total energy consumption is far less than that of iron oxide/hydroxide and bio-magnetite. For calculating this electrolysis energy consumption, the average cell voltage was multiplied by the electrical charge per mass of iron produced. The result is 19.1 MJ/kg, which is also comparable with the estimated energy consumption of 19 MJ/kg for an industrial blast furnace [56]. The microbial iron reduction energy is minimal as *C. ferrireducens* can utilize in situ-produced H_2 from water electrolysis [42]. Accordingly, the energy demand for the bio-enrichment step is estimated at 1.2 MJ/kg, making it a highly efficient approach for upgrading low-grade iron ores.

The SEM images of the highly amorphous and scattered iron oxide/hydroxide vs. the smoother and more uniform surface with agglomerated particles of bio-magnetite confirm the microstructural changes caused by the bio-mineralization process as the cellular components could act as the nucleation points for crystallization (Fig. 5). A further decrease in surface defects and increased agglomeration was achieved by the heat treatment process as it reduced surface irregularity and increased particle cohesion. In addition, the SEM image of a reduced bio-hematite after 20 hours of alkaline electrolysis shows areas where iron is inclusively present as individual phases. The elemental map data for Fe(0) is presented in Supplementary Fig. S-6.

While the recovered iron is not yet 100 % pure, the process is close to full conversion. The presence of minor impurities can be efficiently addressed through straightforward post-processing steps. Once these minor adjustments are made, the iron will be suitable for various applications, including construction, manufacturing, and space exploration. Addressing these challenges through additional processing steps will improve the material's quality, making it viable for broader industrial uses. These additional steps are common in metallurgy and do not detract from the potential of the proposed process for sustainable iron production.

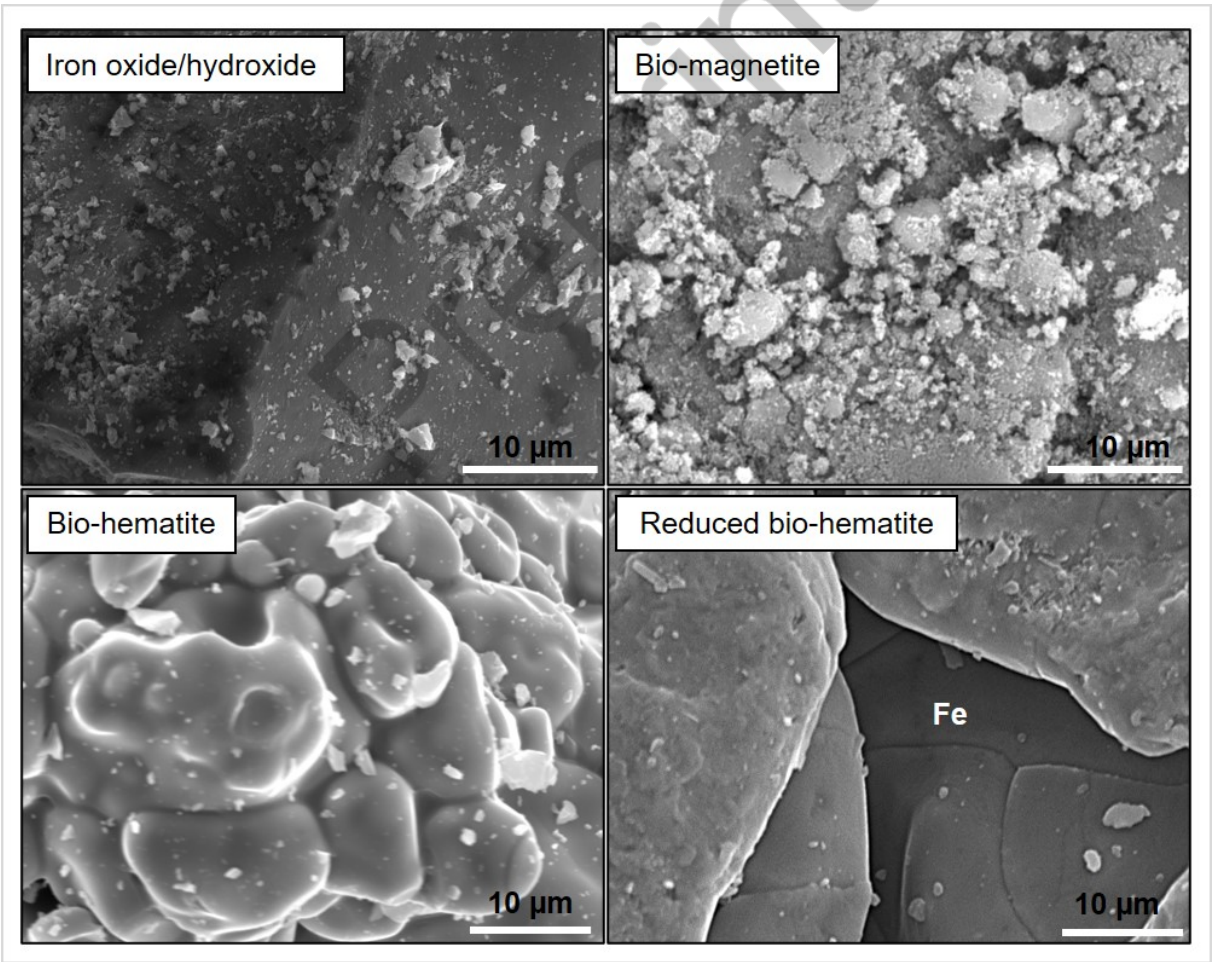

Fig. 5: SEM images of initial iron oxide/hydroxide, bio-magnetite, and bio-hematite (after heat treatment) confirm the microstructural changes during the bio-leaching and heat treatment processes. The image of a reduced bio-hematite after 20 h of electrolysis at -1.4 V vs. Ag/AgCl in 10 M NaOH at 363 K shows areas where Fe is inclusively present.

3.3. Effects of heat treatment and bio-mineralization

To cross-check heat treatment effects on microstructure and reducibility, control tests were conducted. Commercial hematite, with and without heat treatment, was subjected to alkaline electrolysis for 5 h. Commercial and biologically produced magnetite were also compared to gain a better insight into bio-mineralization impacts. The electrolysis plots as well as the corresponding iron extraction yield and Faradaic efficiency, are presented in Fig. 3d. Note that these results are not directly comparable to the 20 h test results due to the different materials and test durations.

First, it can be seen that the reducibility of commercial hematite (both heat-treated and untreated), with its single Fe(III) valence, outperforms commercial magnetite and bio-magnetite, as thermodynamically expected. The relatively less negative Gibbs free energy for these Fe(III) oxides as mentioned above, suggests that under the same electrochemical conditions, they can be reduced to metallic iron more readily.

A comparative analysis of the microstructural properties of non-heat-treated commercial hematite (SSA: 2.6 m^2/g, DC: 95(5) %, ACS: 135(1) nm) and that after heat treatment (SSA: 0.76 m^2/g, DC: 99(5) %, ACS: 173(2) nm) confirms that thermal treatment results in a lower specific surface area and higher ACS (Table 1). Electrochemically, the heat treatment of commercial hematite led to a decline in currents and a higher iron yield and current efficiency. This is further evidence of the influence of crystallinity and grain size on reducibility and side reactions. These observations, in line with the improvements noted in the previous section, corroborate the benefits of heat treatment optimizing iron oxide/hydroxide electrochemical properties.

We also observed a superior reducibility of bio-magnetite compared to a commercial magnetite. We compared commercial magnetite, with SSA of 8.1 m^2/g, DC of 87(5) %, and ACS of 74(1) nm, to bio-magnetite synthesized from the iron oxide/hydroxide in this research, with SSA of 41.5 m^2/g, a DC of 80(5) %, and ACS of 16.2(2) nm. Theoretically, the microstructural properties of commercial magnetite might be expected to confer advantages due to its lower SSA, suggesting fewer active sites and potentially reduced parasitic reactions. Despite this, our results indicated that bio-magnetite demonstrated enhanced electrochemical behavior in terms of iron yield and current efficiency.

EDX analysis revealed traces of carbon in the bio-magnetite sample (Supplementary Fig. S-7), probably from decomposed microorganisms or the partial formation of siderite ($FeCO_3$). It is hypothesized that these organic residues could serve as binding sites to facilitate electron transfer, particularly enhancing iron reduction. The possible presence of siderite embedded within the bio-magnetite matrix could thermodynamically favor the reduction process. Previous studies suggest that the composition of the cultivation medium and specific parameters can influence mineral formation during bio-mineralization, with siderite formation being reported in bicarbonate-buffered media like the one used in this research [54,55]. In particular, thermophilic iron-reducing microorganisms are known to produce mixtures of magnetite and siderite during the reduction of ferrihydrite [59]. Given the complexity of the bio-mineralization process, further studies are needed to confirm these findings fully.

4. Perspective

This research enabled us to identify a future approach for iron fabrication from low-grade iron resources such as the Martian regolith. The MGS-1 basaltic Mars regolith simulant is manufactured from a mixture of several rocks [60]. The composition consists of amorphous and crystalline phases. The composition list includes five iron-containing minerals, namely olivine, hematite, magnetite, ferrihydrite, and Fe-carbonate, as well as their iron contents (Table 2). It is evident that ferrihydrite, the investigated mineral in this study, is the major iron-bearing phase of the Martian regolith.

Key challenges in extraterrestrial iron mining include the variable composition of Martian regolith and the limited availability of consistent energy sources. Martian regolith contains a mix of iron-bearing minerals, complicating extraction, while intermittent solar power requires efficient energy management [61].

Our attempt to reduce regolith directly using alkaline electrolysis at 363 K did not lead to any metal production as aqueous solutions do not provide a high enough potential window to decompose the complicated mixed mineral phases of regolith. Current methods, such as molten regolith electrolysis (~1873 K) and solid-state reduction (~1173 K), face significant challenges, including partial reductions, mixed metal outputs, incomplete oxygen removal, and unselective metal extraction, making them impractical for efficient use. To enable iron recovery using alkaline electrolysis at moderate temperatures, it is necessary to first precipitate the ferrous phases.

We, therefore, see the perspective that with an optimized upstream bio-mineralization beneficiation step, iron-containing phases could be converted to magnetically responsive forms. This property is crucial for isolating iron from the regolith's complex mixture of minerals. An intermediate heat treatment step before electrochemical reduction will also be suggested based on this study. The proposed concept for the fabrication of iron from Martian regolith is represented in Fig. 6. This approach leverages ISRU, minimizing transport costs from Earth. Using Ni/Fe as a non-contaminating inert anode material also aligns with the nickel trace presence in Martian meteorites [62]. We underscore the importance of ongoing research to validate the concept for the MGS-1 Martian regolith simulant.

Table 2. The mineral composition (manufacturer fact sheet) of MGS-1 Martian regolith simulant and the iron content of the iron-bearing phases.

Mineral	Total /wt.%	Iron /wt.%
Crystalline		
Plagioclase	27.1	-
Pyroxene	20.3	-
Olivine	13.7	29.3
Hematite	0.5	5.1
Magnetite	1.9	20.3
Amorphous		
Anhydrite	1.7	-
Basaltic Glass	22.9	-
Hydrated Silica	3.0	-
Mg-sulfate	4.0	-
Ferrihydrite	3.5	35.4
Fe-carbonate	1.4	9.9

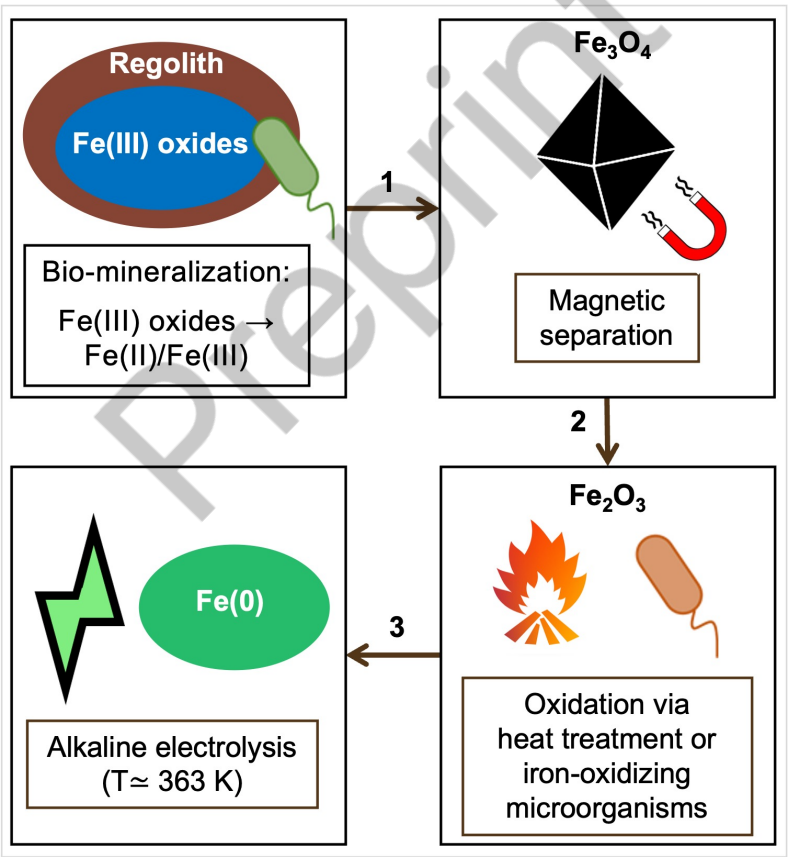

Fig. 6: The proposed concept of alkaline deoxidation electrolysis with upstream bio-mineralization beneficiation and oxidation using thermal treating or iron-oxidizing microorganisms for extraterrestrial iron fabrication from Martian regolith.

Furthermore, further investigations are required to quantify the proportion of microbial cells present in the bio-mineralized minerals and to evaluate their influence on the electrochemical behavior. Depending on the microbial species and the cultivation conditions, iron-reducing microorganisms may rely on different extracellular electron transfer mechanisms and strategies to reduce iron oxides, including direct contact with iron particles or electron shuttles (endogenous or exogenous) for iron reduction at a distance [63]. Likewise, the cultivation medium may include variable amounts of inorganic salts and organic matter, which might be bound to iron oxides [64].
Finally, microorganisms could also replace heat treatment. The idea would be to use iron-oxidizing

microorganisms to bio-transform magnetite into ferric iron oxides such as hematite and maghemite, or to further reduce the magnetite to ferrous iron carbonate (siderite) [61,63,64]. This innovative combination could further decrease energy consumption as it could eliminate the heat treatment step which involves temperatures around 1173 K. Validation of the concept of bio-mineralization of Martian regolith to produce bio-magnetite, magnetic precipitation, and bio-oxidation/reduction (as a substitute for heat treatment) followed by alkaline electrolysis for iron production will be the subject of further studies.

5. Conclusion

This study addresses the challenges associated with the electrochemical reduction of low-grade iron ores by introducing bio-mineralization as a key beneficiation step. Ferrihydrite, a common iron-rich phase, was selected due to its abundance and potential for conversion. Through anaerobic respiration, iron-reducing bacteria convert ferrihydrite into bio-magnetite, allowing for magnetic separation of iron-bearing phases from impurities. This bio-magnetite was then successfully reduced to metallic iron via electrolysis in an alkaline medium at moderate temperatures. This conversion achieved iron yields of 25(1) wt.% with a current efficiency of 9(2) % after 20 hours. Incorporating heat treatment increased the yield to 67(1) wt.% with a current efficiency of 63(3) %. Bio-hematite, with a Fe(III) valence state that is thermodynamically easier to reduce, proved to be more reducible than bio-magnetite, reinforcing the benefits of heat treatment. Additionally, the estimated energy consumption of 19.1 MJ/kg is competitive with current industrial standards, demonstrating the viability of this approach. This study also highlights the importance of microstructure on reducibility. Controlled heat treatment improves crystallinity and reduces active sites for side reactions, such as hydrogen evolution, while facilitating electron flow. However, excessive agglomeration could hinder electrolyte diffusion and oxygen ion release, underscoring the need for precise control of heat treatment parameters [68].
These findings provide a promising, sustainable pathway for iron production from low-grade resources, including potential applications in extraterrestrial environments like Mars, where conventional extraction methods are impractical.
Key takeaways from this work include:

1. Bio-mineralization: Iron-reducing bacteria convert iron-bearing phases into bio-magnetite, enabling future magnetic separation and enrichment of iron in low-grade ores.
2. Electrochemical reduction: Concentrated iron oxides were efficiently reduced to metallic iron using an energy-efficient electrochemical process in an alkaline medium.
3. Environmental sustainability: This method offers a low-energy, low-emission alternative for extracting iron from waste and low-grade resources.
4. Extraterrestrial application: The approach shows promise for iron extraction from Martian regolith, supporting future in-situ resource utilization for space missions.

Looking ahead, while this study demonstrated promising short-term electrochemical stability, the long-term performance of the electrochemical reduction of bio-magnetite and bio-hematite under industrial conditions remains untested. Future work should prioritize validation of the concept for low-grade iron ores such as the Martian regolith simulant. Future efforts will then be required for scaling up, including the cultivation of iron-reducing bacteria, the management of bio-mineralization, and efficient by-product handling. Optimizing bioreactor systems, conducting comprehensive techno-economic analyses, and understanding the kinetics of iron reduction under varying operational conditions will be crucial for the commercial viability and industrial scalability of this process.

Data availability

All measurement data that are included in this publication are uploaded to an online repository [69] along with Python scripts to evaluate the data and generate the plots of this study.

Author contributions statement

R.F., F.L.M., M.B., A.C., G.P., S.K., and J.T. conceived the concept. R.F. conducted the electrochemical experiments and coordinated the overall workflow. F.L.M., M.B., and J.T. supervised the electrochemical part. A.C. performed the biological experiments. G.P. and S.K. supervised the biological work. Sample characterization was conducted by M.I.J.H. under the supervision of T.M.G. The manuscript was mainly written by R.F. All authors analyzed and discussed the results and revised the manuscript.

Funding

This project is part of the 'Humans on Mars Initiative' funded by the Federal State of Bremen and the University of Bremen.
For details on the projects, refer to
Humans on Mars - Pathways to a long-term sustainable human presence
Learning from Mars to preserve Earth
https://www.uni-bremen.de/en/aerospace-at-the-university-of-bremen/humans-on-mars

Acknowledgments

The authors would like to thank Lucio Colombi Ciacchi for suggesting this research.

Declaration of competing interest
The authors declare no competing interests.

Supporting information
The supplementary material is stored in a repository available at
https://doi.org/10.5281/zenodo.13283858

Correspondence and requests for materials should be addressed to J.T.

References

1. Oarga-Mulec A, Luin U, Valant M (2024) Back to the future with emerging iron technologies. RSC Adv 20765–20779. https://doi.org/10.1039/d4ra03565h
2. Kim J, Sovacool BK, Bazilian M, et al (2022) Decarbonizing the iron and steel industry: A systematic review of sociotechnical systems, technological innovations, and policy options. Energy Res Soc Sci 89:102565. https://doi.org/10.1016/j.erss.2022.102565
3. Wang X, Yang H, Yu X, et al (2023) Research progress in the preparation of iron by electrochemical reduction route without CO2 emissions. J Appl Electrochem 53:1521–1536. https://doi.org/10.1007/s10800-023-01870-7
4. Ranzani Da Costa A, Wagner D, Patisson F, et al (2013) Modelling a new, low CO2 emis-sions, hydrogen steelmaking process. J Clean Prod 46:27–35. https://doi.org/10.1016/j.jclepro.2012.07.045ï
5. Fayaz R, Bösing I, La Mantia F, et al (2023) Deoxidation Electrolysis of Hematite in Alkaline Solution: Impact of Cell Configuration and Process Parameters on Reduction Efficiency. ChemElectroChem 10:1–9. https://doi.org/10.1002/celc.202300451
6. Jovičević-Klug M, Souza Filho IR, Springer H, et al (2024) Green steel from red mud through climate-neutral hydrogen plasma reduction. Nature 625:703–709. https://doi.org/10.1038/s41586-023-06901-z
7. Wang RR, Zhao YQ, Babich A, et al (2021) Hydrogen direct reduction (H-DR) in steel industry—An overview of challenges and opportunities. J Clean Prod 329:129797. https://doi.org/10.1016/j.jclepro.2021.129797
8. UN (2024) Progress towards the Sustainable Development Goals, Report of the Secretary-General. Assembly 64782:14
9. Ganiyu SO, Martínez-Huitle CA (2020) The use of renewable energies driving electrochemical technologies for environmental applications. Curr Opin Electrochem 22:211–220. https://doi.org/10.1016/j.coelec.2020.07.007
10. Hecht M, Hoffman J, Rapp D, et al (2021) Mars Oxygen ISRU Experiment (MOXIE). Space Sci Rev 217:. https://doi.org/10.1007/s11214-020-00782-8
11. Childs CW (1992) Ferrihydrite: A review of structure, properties and occurrence in relation to soils. Soil Conservation
12. Filip J, Zboril R, Schneeweiss O, et al (2007) Environmental applications of chemically pure natural ferrihydrite. Environ Sci Technol 41:4367–4374. https://doi.org/10.1021/es062312t
13. Bazylinski DA, Frankel RB, Konhauser KO (2007) Modes of biomineralization of magnetite by microbes. Geomicrobiol J 24:465–475. https://doi.org/10.1080/01490450701572259
14. Ehlmann BL, Edwards CS (2014) Mineralogy of the Martian surface. Annu Rev Earth Planet Sci 42:291–315. https://doi.org/10.1146/annurev-earth-060313-055024
15. Hinterman E (2020) Simulating oxygen production on Mars for the Mars Oxygen In-Situ Resource Utilization Experiment. Acta Astronaut 170:678–685. https://doi.org/10.1016/j.actaastro.2020.02.043
16. Schlüter L, Cowley A (2020) Review of techniques for In-Situ oxygen extraction on the moon. Planet Space Sci 181:104753.

https://doi.org/10.1016/j.pss.2019.104753
17. Humbert MS, Brooks GA, Duffy AR, et al (2022) Thermophysical property evolution during molten regolith electrolysis. Planet Space Sci 219:105527. https://doi.org/10.1016/j.pss.2022.105527
18. Schreiner SS, Sibille L, Dominguez JA, Hoffman JA (2016) A parametric sizing model for Molten Regolith Electrolysis reactors to produce oxygen on the Moon. Advances in Space Research 57:1585–1603. https://doi.org/10.1016/j.asr.2016.01.006
19. Meurisse A, Lomax B, Selmeci Á, et al (2022) Lower temperature electrochemical reduction of lunar regolith simulants in molten salts. Planet Space Sci 211:. https://doi.org/10.1016/j.pss.2021.105408
20. Bösing I, La Mantia F, Thöming J (2022) Modeling of electrochemical oxide film growth-a PDM refinement. Electrochim Acta 406:. https://doi.org/10.1016/j.electacta.2022.139847
21. Monteiro JF, Ivanova YA, Kovalevsky A V., et al (2016) Reduction of magnetite to metallic iron in strong alkaline medium. Electrochim Acta 193:284–292. https://doi.org/10.1016/j.electacta.2016.02.058
22. Feynerol V, Lavelaine H, Marlier P, et al (2017) Reactivity of suspended iron oxide particles in low temperature alkaline electrolysis. J Appl Electrochem 47:1339–1350. https://doi.org/10.1007/s10800-017-1127-5
23. Lopes D V., Lisenkov AD, Sergiienko SA, et al (2021) Alkaline Electrochemical Reduction of a Magnesium Ferrospinel into Metallic Iron for the Valorisation of Magnetite-Based Metallurgical Waste. J Electrochem Soc 168:073504. https://doi.org/10.1149/1945-7111/ac1490
24. Maihatchi A, Pons MN, Ricoux Q, et al (2020) Electrolytic iron production from alkaline suspensions of solid oxides: Compared cases of hematite, iron ore and iron-rich bayer process residues. Journal of Electrochemical Science and Engineering 10:95–102. https://doi.org/10.5599/jese.751
25. Lopes D V., Lisenkov AD, Ruivo LCM, et al (2022) Prospects of Using Pseudobrookite as an Iron-Bearing Mineral for the Alkaline Electrolytic Production of Iron. Materials 15:1–19. https://doi.org/10.3390/ma15041440
26. Maihatchi Ahamed A, Pons MN, Ricoux Q, et al (2020) Production of electrolytic iron from red mud in alkaline media. J Environ Manage 266:. https://doi.org/10.1016/j.jenvman.2020.110547
27. Johnson DB (2014) Biomining-biotechnologies for extracting and recovering metals from ores and waste materials. Curr Opin Biotechnol 30:24–31. https://doi.org/10.1016/j.copbio.2014.04.008
28. Gumulya Y, Zea L, Kaksonen AH (2022) In situ resource utilisation: The potential for space biomining. Miner Eng 176:107288. https://doi.org/10.1016/j.mineng.2021.107288
29. Cockell CS, Santomartino R, Finster K, et al (2020) Space station biomining experiment demonstrates rare earth element extraction in microgravity and Mars gravity. Nat Commun 11:1–11. https://doi.org/10.1038/s41467-020-19276-w
30. Volger R, Pettersson GM, Brouns SJJ, et al (2020) Mining moon & mars with microbes: Biological approaches to extract iron from Lunar and Martian regolith. Planet Space Sci 184:104850. https://doi.org/10.1016/j.pss.2020.104850
31. Castelein SM, Aarts TF, Schleppi J, et al (2021) Iron can be microbially extracted from Lunar and Martian regolith simulants and 3D printed into tough structural materials. PLoS One 16:1–21. https://doi.org/10.1371/journal.pone.0249962
32. Viollier E, Inglett PW, Hunter K, et al (2000) The Ferrozine method revisted. Applied Geochemistry 15:785–790
33. Wang S lan, Haarberg GM, Kvalheim E (2008) Electrochemical Behavior of Dissolved Fe2O3 in Molten CaCl2-KF. Journal of Iron and Steel Research International 15:48–51. https://doi.org/10.1016/S1006-706X(08)60265-4
34. Trotochaud L, Young SL, Ranney JK, Boettcher SW (2014) Nickel-Iron

oxyhydroxide oxygen-evolution electrocatalysts: The role of intentional and incidental iron incorporation. J Am Chem Soc 136:6744–6753. https://doi.org/10.1021/ja502379c
35. Hyslop DJS, Abdelkader AM, Cox A, Fray DJ (2010) Utilization of Constant Current Chronopotentiometry to Synthesize a Co–Cr Alloy. J Electrochem Soc 157:E111. https://doi.org/10.1149/1.3427511
36. Qiao J, Liu Y, Hong F, Zhang J (2014) A review of catalysts for the electroreduction of carbon dioxide to produce low-carbon fuels. Chem Soc Rev 43:631–675. https://doi.org/10.1039/c3cs60323g
37. Gesing TM, Robben L (2024) Determination of the average crystallite size and the crystallite size distribution: The envelope function approach EnvACS. J Appl Crystallogr. https://doi.org/10.1107/S1600576724007362
38. Slobodkin A, Reysenbach AL, Strutz N, et al (1997) Thermoterrabacterium ferrireducens gen. nov., sp. nov., a thermophilic anaerobic dissimilatory Fe(III)-reducing bacterium from a continental hot spring. Int J Syst Bacteriol 47:541–547. https://doi.org/10.1099/00207713-47-2-541
39. Gavrilov SN, Zavarzina DG, Elizarov IM, et al (2021) Novel Extracellular Electron Transfer Channels in a Gram-Positive Thermophilic Bacterium. Front Microbiol 11:1–21. https://doi.org/10.3389/fmicb.2020.597818
40. Verseux C, Baqué M, Lehto K, et al (2016) Sustainable life support on Mars - The potential roles of cyanobacteria. Int J Astrobiol 15:65–92. https://doi.org/10.1017/S147355041500021X
41. Verseux C, Heinicke C, Ramalho TP, et al (2021) A Low-Pressure, N2/CO2 Atmosphere Is Suitable for Cyanobacterium-Based Life-Support Systems on Mars. Front Microbiol 12:1–15. https://doi.org/10.3389/fmicb.2021.611798
42. Gavrilov SN, Bonch-Osmolovskaya EA, Slobodkin AI (2003) Physiology of organotrophic and lithotrophic growth of the thermophilic iron-reducing bacteria Thermoterrabacterium ferrireducens and Thermoanaerobacter siderophilus. Microbiology (N Y) 72:132–137. https://doi.org/10.1023/A:1023299410478
43. Slobodkin AI (2005) Thermophilic microbial metal reduction. Mikrobiologiya 74:581–595
44. Vandieken V, Mußmann M, Niemann H, Jørgensen BB (2006) Desulfuromonas svalbardensis sp. nov. and Desulfuromusa ferrireducens sp. nov., psychrophilic, Fe(III)-reducing bacteria isolated from Arctic sediments, Svalbard. Int J Syst Evol Microbiol 56:1133–1139. https://doi.org/10.1099/ijs.0.63639-0
45. Kashefi K, Lovley DR (2003) Extending the upper temperature limit for life. Science (1979) 301:934. https://doi.org/10.1126/science.1086823
46. Beveridge TJ, Murray RGE (1980) Sites of metal deposition in the cell wall of Bacillus subtilis. J Bacteriol 141:876–887. https://doi.org/10.1128/jb.141.2.876-887.1980
47. Fein JB (2000) Quantifying the effects of bacteria on adsorption reactions in water-rock systems. Chem Geol 169:265–280. https://doi.org/10.1016/S0009-2541(00)00207-2
48. Sk MM, Pradhan P, Patra BK, Guria AK (2023) Green biomass derived porous carbon materials for electrical double-layer capacitors (EDLCs). Mater Today Chem 30:. https://doi.org/10.1016/j.mtchem.2023.101582
49. Green DW, Perry RH (2008) Perry's Chemical Engineers' Handbook, Eighth Edi. McGraw-Hill
50. Zou X, Gu S, Lu X, et al (2015) Electroreduction of Iron(III) Oxide Pellets to Iron in Alkaline Media: A Typical Shrinking-Core Reaction Process. Metallurgical and Materials Transactions B: Process Metallurgy and Materials Processing Science 46:1262–1274. https://doi.org/10.1007/s11663-015-0336-8
51. Heidari A, Niknahad N, Iljana M, Fabritius T (2021) A review on the kinetics of iron ore reduction by hydrogen. Materials 14:.

https://doi.org/10.3390/ma14247540
52. Spreitzer D, Schenk J (2019) Reduction of Iron Oxides with Hydrogen—A Review. Steel Res Int 90:. https://doi.org/10.1002/srin.201900108
53. Zhang L, Wu H Bin, Lou XW (2014) Iron-oxide-based advanced anode materials for lithium-ion batteries. Adv Energy Mater 4:1–11. https://doi.org/10.1002/aenm.201300958
54. Pervez SA, Kim D, Farooq U, et al (2014) Comparative electrochemical analysis of crystalline and amorphous anodized iron oxide nanotube layers as negative electrode for LIB. ACS Appl Mater Interfaces 6:11219–11224. https://doi.org/10.1021/am501370f
55. Aeppli M;, Voegelin A;, Gorski CA;, et al (2018) Mediated Electrochemical Reduction of Iron (Oxyhydr-)Oxides under Defined Thermodynamic Boundary Conditions. Environ Sci Technol 52(2):560–570. https://doi.org/10.3929/ethz-b-000235669
56. Sohn HY, Mohassab Y (2016) Greenhouse Gas Emissions and Energy Consumption of Ironmaking Processes
57. Zachara JM, Kukkadapu RK, Fredrickson JK, et al (2002) Biomineralization of poorly crystalline Fe(III) oxides by dissimilatory metal reducing bacteria (DMRB). Geomicrobiol J 19:179–207. https://doi.org/10.1080/01490450252864271
58. Dong H, Fredrickson JK, Kennedy DW, et al (2000) Mineral transformation associated with the microbial reduction of magnetite. Chem Geol 169:299–318. https://doi.org/10.1016/S0009-2541(00)00210-2
59. Piepenbrock A, Dippon U, Porsch K, et al (2011) Dependence of microbial magnetite formation on humic substance and ferrihydrite concentrations. Geochim Cosmochim Acta 75:6844–6858. https://doi.org/10.1016/j.gca.2011.09.007
60. Cannon KM, Britt DT, Smith TM, et al (2019) Mars global simulant MGS-1: A Rocknest-based open standard for basaltic martian regolith simulants. Icarus 317:470–478. https://doi.org/10.1016/j.icarus.2018.08.019
61. Ganiyu SO, Martínez-Huitle CA, Rodrigo MA (2020) Renewable energies driven electrochemical wastewater/soil decontamination technologies: A critical review of fundamental concepts and applications. Appl Catal B 270:118857. https://doi.org/10.1016/j.apcatb.2020.118857
62. Kong P, Ebihara M, Palme H (1999) Siderophile elements in Martian meteorites and implications for core formation in Mars. Geochim Cosmochim Acta 63:1865–1875. https://doi.org/10.1016/S0016-7037(99)00030-7
63. Nevin KP, Lovley DR (2002) Mechanisms for Fe(III) oxide reduction in sedimentary environments. Geomicrobiol J 19:141–159. https://doi.org/10.1080/01490450252864253
64. Cornell RM, Schwertmann U (2003) Adsorption of Ions and Molecules
65. Weber KA, Achenbach LA, Coates JD (2006) Microorganisms pumping iron: Anaerobic microbial iron oxidation and reduction. Nat Rev Microbiol 4:752–764. https://doi.org/10.1038/nrmicro1490
66. Brown A.* D, Sherrif L. B, Sawicki A. J (1997) Microbial transformation of magnetite to hematite. Geochim Cosmochim Acta 61:3341–3348
67. Ohenhen LO, Feinberg JM, Slater LD, et al (2022) Microbially Induced Anaerobic Oxidation of Magnetite to Maghemite in a Hydrocarbon-Contaminated Aquifer. J Geophys Res Biogeosci 127:1–24. https://doi.org/10.1029/2021JG006560
68. Chen GZ, Gordo E, Fray DJ (2004) Direct electrolytic preparation of chromium powder. Metallurgical and Materials Transactions B: Process Metallurgy and Materials Processing Science 35:223–233. https://doi.org/10.1007/s11663-004-0024-6
69. R. Fayaz, (2024). Data Availability. Zenodo. https://doi.org/10.5281/zenodo.13284391